DOI: https://doi.org/10.15407/techned2025.05.009

QUASI-STATIC MODEL OF RESONANT POWER CONVERTER

G.V. Pavlov[1], A.V. Obrubov[2], I.L. Vinnichenko[3], A.O. Makhnov[4]
Admiral Makarov National University of Shipbuilding,
Heroiv Ukrayiny Ave.9, Mykolaiv, 54007, Ukraine,
e-mail: pavlov.gv.nuk@gmail.com; andrii.obrubov@nuos.edu.ua; i.l.vinnychenko@gmail.com; andrei.schneidereu@gmail.com.

In this paper, a quasi-static model of the resonant power converter with inverter, LLC circuit, and diode rectifier is obtained, which is a linear mathematical model derived from the analysis of quasi-steady-state processes of the substitution circuit for constant values of input and output signals. The quasi-static model is determined on the basis of the dynamic model of the resonant converter for infinite time, which made it possible to obtain analytical expressions of static characteristics based on transient functions. As a result of calculations based on the quasi-static model, the family of static characteristics of the resonant converter, which is replaced by the structure with equivalent voltage generators and a passive part of the circuit, is obtained. The passive part contains the resonant circuit, the voltage transformer, and some parasitic parameters of the transformer and other circuit elements. Equivalent voltage generators replace the voltage inverter with the power source and the rectifier with the load. Thus, the switched power circuit of the resonant converter is replaced by the non-switched circuit with voltage generators and the passive multipole. The input values of the substitution circuit are the voltages of equivalent generators, and their currents are the output values. Quasi-steady-state processes are represented as a set of stationary functions consisting of stationary transient functions. Stationary functions are the sum of individual transient functions that repeat from period to period of the operating frequency. To determine the transient functions according to the finite value theorem of the z-image, we use the transfer functions obtained from the discrete dynamic model of the resonant converter. The algorithm for switching power valves is taken into account when formulating the steady-state current formula of the output equivalent generator, at the intervals of non-zero voltage of which the average load current is determined by integrating the steady-state current. Comparison of the calculated static characteristics with the experimental characteristics confirmed the correctness of the theoretical results. References 24, figures 6, table 1.
Keywords: resonant converter, quasi-static model, stationary function, transient function.

Introduction. The topic of calculating the parameters of quasi-steady-state modes [1, 2] and determining the static characteristics of resonant power converters (**RPCs**) has already been widely considered in [3, 4], since static characteristics provide the necessary information on the possible ranges of input and output values of RPCs during long-term operation. The results of further research in this direction made it possible to approach more general principles of creating the quasi-static model of the RPC. Since the RPC is a pulse system of periodic action, the processes in it can be divided into conditionally constant and oscillating components [5, 6]. This approach allows to perform the detailed analysis of electromagnetic processes in the power part of the resonant pulse semiconductor converters [7], that leads to the possibility of control adjustment to provide, for example, the desired sinusoidal output voltage with the close to zero total harmonic distortion [8]. Conditionally constant components of processes can be constant while the RPC is able to operate normally. For example, the inverter supply voltage can be constant when connected to an ideal power source. The RPC output load voltage in case of the ideal filtering or in case of the load being the ideal voltage source, can also be constant. In the dynamic modes, the conditionally constant components can change during the operation of the RPC, for instance, the slowly changing output voltage during the inter-commutation intervals [9]. Usually, the changing rate of the conditionally constant components is low

ORCID: [1] https://orcid.org/0000-0002-4937-1828; [2] https://orcid.org/0000-0001-9667-1703;
[3] https://orcid.org/0000-0002-3768-1060; [4] https://orcid.org/0009-0006-1755-7405

compared to the changing rate of the oscillating components [10, 11]. Oscillating components, which include voltages and currents of the oscillating circuit elements, high-frequency transformer, etc., cannot be constant in RPC operating modes according to the principle of operation of the inverter, transformer, and rectifier [12, 13]. Therefore, as the quasi-static model of the RPC the authors consider the mathematical model that describes processes when their conditionally constant components are really constant values, and oscillatory components are stationary variable values, i.e., periodically repeated [10, 14, 15].

The aim of the study is to create a quasi-static model of the RPC, which will allow to calculate the theoretical static characteristics and determine the changing ranges in the output values.

1. Problem statement. Compared to purely experimental approach to determining characteristics (for example, multiple experiments with *SIMULINK* models or using an RPC sample), the use of a quasi-static model allows to quickly determine the achievable limits of the RPC output values and dependencies for different parameters of the power circuit. The object of modelling is the RPC with the circuit in Fig. 1, *a*, containing: a voltage inverter (Inv); a resonant *LLC-circuit* with the high-frequency transformer (*TV*), combined into the passive part (PP) on Fig. 1, *b*; a bridge rectifier (Rec); a filter capacitance (C_q) with connected active load (R_q). The local control system (LCS) generates all the necessary signals for the inverter operation using the signals of the circuit current sensor (*cs1*) and the resonant capacitor voltage sensor (*vs1*) [12, 13, 16]. The output power of the RPC is regulated by the intermediate signal U_{reg} from the automatic regulator (AR). The rectified current and load voltage are measured using the *cs2* and *vs*2 sensors. In quasi-steady-state operation, the supply voltage U_s, the regulator voltage U_{reg}, the load voltage U_q and the operating frequency ω_g are constant. The operating frequency of the RPC with automatic frequency control [14, 15] and with auto-generation [23] in certain load ranges can also be considered constant. The structural diagram in Fig. 1, *b* reflects the cause-and-effect relationships in the circuit in Fig. 1, *a*. The supply voltage U_s determines the amplitude of the rectangular voltage u_g at the output of the equivalent generator (EG1), which simulates a voltage inverter. The load voltage U_q determines the amplitude of the voltage u_b at the output of the equivalent generator (EG2), which simulates a rectifier. Both voltages u_g and u_b are input values of the passive part. The output values of the passive part are the current at the output of the inverter i_g and the current at the input of the rectifier i_b. If the load of the RPC is resistance R_q, then in the circuit in Fig. 1, *b* there will be a feedback $U_q=I_q(I_{sb})\cdot R_q$.

The following assumptions were made when constructing the quasi-static RPC model. Switching processes are assumed to be instantaneous. The inverter and rectifier switches are perfect. The power supply and load are replaced by voltage sources. The *TV* transformer is linear. The resonant elements L_r, C_r and other passive elements (L_{s1}, L_{s2}, L_{m1}, L_{m2}) are included into the four-pole passive part in Fig. 1, *b*.

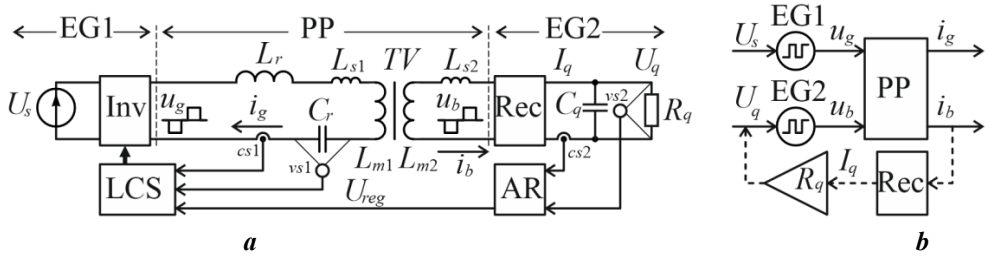

a ***b***

Fig. 1

The input data for the quasi-static model of the RPC are: the circuit and parameters of the passive part elements; the operating frequency ω_g; the amplitudes and shapes of the steady-state voltages of the equivalent generators u_g and u_b. The output values are functions of steady-state currents input I_{sg} and output I_{sb}, according to the input and output currents (i_g and i_b) of the passive part of the RPC, and the average rectified current I_q.

Thus, in order to build the quasi-static model of the RPC, the following tasks need to be solved:

- Determination of steady-state currents $I_{s\ldots N}$ depending on the passive part structure and parameters.
- Matching the phase shift of the voltages of equivalent generators.
- Creation of the formula for the steady-state current of the output equivalent generator, taking into account the switching functions depending on the sequence of source combinations [4].
- Calculation of the average load current I_q depending on the switching algorithm of the RPC switches and the filtering method.

2. Determination of the steady-state current. The steady-state current $I_{skj}(\sigma+x_j)$ of the k-th equivalent generator of the RPC replacement circuit with N generators, similar to the circuit in Fig. 1, *b*, is written as the sum of N components – the currents caused separately by each j-th equivalent generator

$$I_{sk}(\sigma \pm x_{sk}) = I_{sk}(\sigma \pm f(x_1 \ldots x_N)) = \sum_{j=1\ldots N} I_{skj}(\sigma \pm x_j), \quad (1)$$

where: k is the index of the generator-current receiver; j is the index of the generator-current source; $\sigma = 0...1$ is the relative time within the period of the operating frequency; x_j is the relative displacement of the current component in time, which is the distance between the beginning of the period of the conversion frequency and the intersection of the current curve with the zero value. The relative displacements x_j of each j-th component of the steady-state current determine the total relative displacement of the steady-state current $x_{sk}=f(x_1 \ldots x_N)$. The voltage of the k-th equivalent oscillator $u_{gk}(\sigma)$ in Fig. 2, *a* (diagram *1*) with a relative width $\gamma_j=0 \ldots 0.5$ in fractions of the period of the operating frequency $T=2\cdot\pi/\omega_g$ has a constant amplitude U_k, frequency ω_g and zero phase shift. The voltage of the j-th equivalent generator $u_{gj}(\sigma-x_j)$ in Fig. 2, *a* (diagram *2*) with amplitude U_j, frequency ω_g and phase $2\pi x_k$ causes a current through the k-th equivalent generator

$$I_{skj}(\sigma - x_j) = U_j\left(\Phi_{kj}(\sigma, x_j) - \Phi_{kj}(\sigma, \gamma_j + x_j) - \Phi_{kj}(\sigma, 0.5 + x_j) + \Phi_{kj}(\sigma, 0.5 + \gamma_j + x_j)\right), \quad (2)$$

where the four terms in the brackets on the right-hand side are stationary functions $\Phi_{kj}(\sigma, x)$, corresponding to the four step voltage components of the j-th equivalent generator $u_{gj}(\sigma-x_j)$ (diagrams *2–4* in Fig. 2, *a*). The voltage components can be considered as separate equivalent voltage generators connected in series to the passive part input. At $j = k$, the current component will belong to the equivalent generator which voltage caused this current.

Fig. 2 shows the process diagrams of the quasi-static model: *a*) voltage diagrams of the j-th equivalent generator and its components; *b*) diagrams of the stationary transient function $g_{skj}(\sigma+1-\delta)$ and the stationary current function $\Phi_{kj}(\sigma,\delta)$ for the j-th input and k-th output of the passive part (1); step voltage function (2); pulse switching functions (3) and (4). Here γ_j is the width of the voltage pulses of the j-th equivalent generator; σ, δ are relative values in fractions of the operating period T.

Fig. 2, *b* shows the diagrams of the stationary process that explain the definition of the stationary function. The time points t_n, t_{n+1} with a constant period of the operating frequency T are fixed ones. The relative offset parameter $\delta = 0...1$ can change with variations in the voltage phase of the equivalent generator. Therefore, the time moments $t_{n-1}+\delta\cdot T$, $t_n+\delta\cdot T$, $t_{n+1}+\delta\cdot T$ can be shifted left and right relatively to the reference points within each period. According to the properties of stationary processes, the stationary function $\Phi_{kj}(\sigma, x)$ in graph (1) of Fig. 2, *b* has the same values at points *a*1, *a*2, *a*3… and slightly smaller values at points *b*1, *b*2...

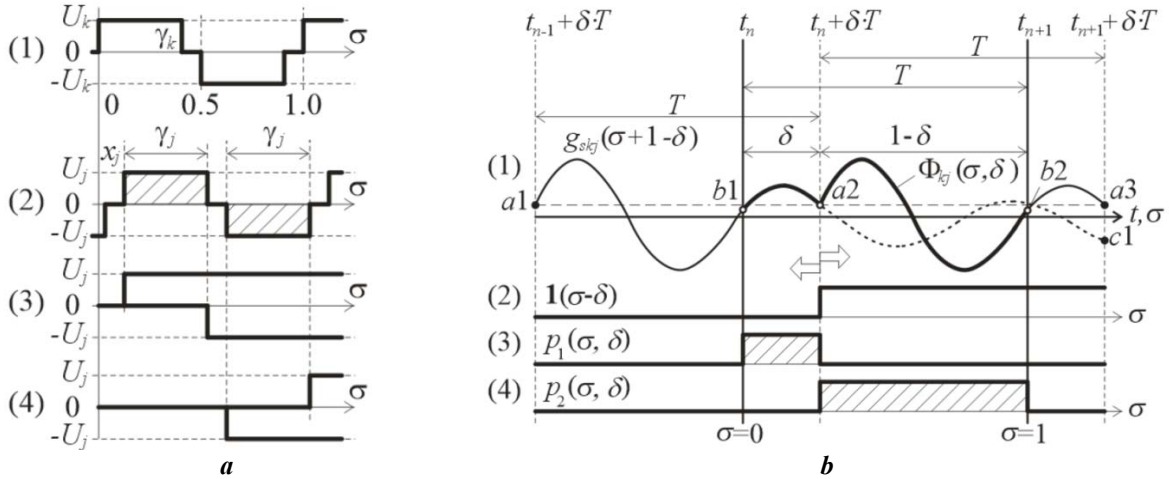

a *b*

Fig. 2

Diagram (1) of Fig. 2, *b* shows the diagrams of the stationary transient function $g_{skj}(\sigma+\alpha)$ (points *a*1-*c*1) and the stationary function $\Phi_{kj}(\sigma,\delta)$, determined during the period of the operating frequency T for two variables: the first $\delta = 0 \ldots 1$ is the voltage offset of the j-th equivalent generator $u_{gj}(\sigma-\delta)=\mathbf{1}(\sigma-\delta)$, shown in diagram (2) of Fig. 2, *a*; the second $\sigma=0...1$ is the relative fraction of the period of the operating frequency T.

The stationary transient function $g_{skj}(\sigma)$ is the current of the k-th equivalent generator caused by the unit voltage of the j-th equivalent generator and for a series resonant LC-circuit is determined on the basis of expressions in the form [16, 22]

$$g(\sigma) = K_I \cdot e^{-\lambda \cdot \sigma} \cdot \sin(\omega_1 \cdot \sigma), \tag{3}$$

where $K_I=\omega_0/(\rho\cdot\omega_1)$, $\lambda=R/(2\cdot L)=\omega_0/(2\cdot Q_0)=\omega_1\cdot\ln(A_k/A_{k+1})/(2\cdot\pi)$ is the oscillations damping factor; A_k, A_{k+1} are the amplitudes of neighbour oscillations; $\omega_0=1/\sqrt{(L\cdot C)}$ is the resonance frequency, rad/s; $\omega_1=\omega_0\cdot\sqrt{(1-1/(4\cdot Q_0^2))}$ is the frequency of free oscillations, rad/s; $Q_0=\rho/r$ is the Q-factor of the circuit; $\rho=\sqrt{(L/C)}$ is the wave impedance of the circuit, Ohm.

The steady-state transient function, refers to the forced component of processes in the steady-state mode, which for the RPC, as a pulse-actuated system, consists of identical periodic transients. Thus, the steady-state transient function $g_{skj}(\sigma)$ is the sum of identical transient functions $g_{kj}(t)$, caused by a sequence of identical voltage pulses. Based on this, the quasi-static RPC model is an extreme variant of the dynamic RPC model for the constant input value and time, which tends to infinity. A single input voltage step of the equivalent oscillator is considered to be an elementary unit pulse of the discrete dynamic RPC model (i.e., it is replaced by the conditionally discrete δ-pulse). The image of the transient function $G_{kj}(z,m)$ will correspond to the transfer function of the passive part for the input from the j-th equivalent generator and the output from the k-th equivalent generator for the input value in the form of the sequence of voltage steps. The original passive part transfer function (3) can be written for the discrete time as

$$g_{kj}(nT, \sigma-\delta) = K_I \cdot e^{-\lambda\cdot T\cdot(n+\sigma-\delta)} \cdot \sin(\omega_1 \cdot T \cdot (n+\sigma-\delta)), \tag{4}$$

then the discrete image (4) will have the form

$$G_{kj}(z,m) = K_I \cdot \frac{e^{-\lambda\cdot m\cdot T}\left(z^2 \cdot \sin(\omega_1 \cdot m \cdot T) + z \cdot e^{-\lambda\cdot T} \cdot \begin{pmatrix} \cos(\omega_1 \cdot m \cdot T)\cdot\sin(\omega_1 \cdot T) - \\ -\sin(\omega_1 \cdot m \cdot T)\cdot\cos(\omega_1 \cdot T) \end{pmatrix}\right)}{z^2 - 2\cdot z\cdot e^{-\lambda\cdot T}\cdot\cos(\omega_1\cdot T) + e^{-2\cdot\lambda\cdot T}}, \tag{5}$$

where $m=\sigma-\delta$. The stationary transition function can be determined by the theorem on the finite value of the discrete z-image of the transition function (5)

$$g_{skj}(\sigma-\delta) = \lim_{z\to 1}\left\{((z-1)/z)\cdot G_{kj}(z,m)\cdot z/(z-1)\right\} =$$

$$= K_I \cdot \frac{e^{-\lambda\cdot m\cdot T}\cdot\sin(\omega_1\cdot\sigma\cdot T) + e^{-\lambda\cdot T\cdot(m+1)}\cdot\begin{pmatrix}\cos(\omega_1\cdot\sigma\cdot T)\cdot\sin(\omega_1\cdot T) - \\ -\sin(\omega_1\cdot\sigma\cdot T)\cdot\cos(\omega_1\cdot T)\end{pmatrix}}{1 - 2\cdot e^{-\lambda\cdot T}\cdot\cos(\omega_1\cdot T) + e^{-2\cdot\lambda\cdot T}}, \tag{6}$$

where the multiplier $z/(z-1)$ on the right-hand side of $G_{kj}(z,m)$ is a representation of the sequence of conditional unit δ-pulses - voltage stages of the j-th equivalent generator. It should be noted that the passive part transient functions for the power source side ($g_{s11}(\sigma)$ i $g_{s12}(\sigma)$) and for the energy consumer side ($g_{s21}(\sigma)$ and $g_{s22}(\sigma)$) may differ from each other.

The stationary function consists of sections of the stationary transient function of the passive part (thickened line between points $b1$-$a2$ and $a2$-$b2$ in Fig. 2, b)

$$\Phi_{kj}(\sigma,\delta) = g_{skj}(\sigma+1-\delta)\cdot p_1(\sigma,\delta) + g_{skj}(\sigma-\delta)\cdot p_2(\sigma,\delta), \tag{7}$$

where the stationary transition function $g_{skj}(x)$ in the simple case corresponds to (6), or will have other expressions for more complex contours [22]. Windowed switching functions $p_1(\sigma, x)$ and $p_2(\sigma, -\delta)$ in diagrams (3) – (4) of Fig. 2, a represent the **п**-pulses determined over the period of the operating frequency for two relative arguments: $p_1(\sigma, \delta) = \mathbf{1}(\sigma)–\mathbf{1}(\sigma–\delta)$, $p_2(\sigma, \delta) = \mathbf{1}(\sigma–\delta)–\mathbf{1}(\sigma–1)$. The first window function $p_1(\sigma, \delta)$ is used to determine the fraction of the stationary function within the period of the operating frequency to the voltage edge of the equivalent generator (points $b1$-$a2$). The second window function $p_2(\sigma, \delta)$ is similarly used after the voltage front (points $a2$-$b2$).

To determine the steady-state current of the k-th equivalent generator $I_{kj}(\sigma\text{-}x_{sk})$, it is necessary to determine the steady-state functions $\Phi_{kj}(\sigma,\delta)$ for each of the possible j in the form (7), i.e. for N equivalent generators. Thus, the steady-state current expression will contain at least 2-N transient functions for N equivalent generators of the RPC replacement circuit, taking into account at least one positive and one negative voltage step of each equivalent generator.

3. Matching the phase shift of the voltages of equivalent generators. Fig. 3 shows the diagrams of the inverter voltage u_g (diagram *1*) and the rectifier input voltage u_b (diagram *2*) with a mismatched phase, since the stationary input current of the rectifier I_b is not exactly opposite to the input voltage. The task of matching the phases of the equivalent generators of the RPC replacement circuit is reduced to determining such a variable offset v between the voltage pulses of the first and second equivalent generators (EG1 and EG2 in Fig. 1, *b*), when the processes in the RPC replacement circuit will be identical to those in the RPC power circuit in Fig. 1, *a*. The voltage of the first equivalent generator u_g is located at the initial position of the time diagram with zero offset. The offset is counted from the beginning of the period of the operating frequency T to the edge of the voltage pulse. The voltage and current of the second equivalent oscillator u_b must be out of phase, similar to the input voltage and current of the diode rectifier RPC operating at voltage U_q. This is illustrated by the diagrams of the matched input voltage u'_b and current I'_b of the diode rectifier in Fig. 3, from which it obviously follows that the resulting phase shift of the steady-state current of the second equivalent generator I_{s2} must be equal to the variable shift of its voltage $x_{s2}=v$, $u'_b = u_b(\sigma-v)=u_{g2}(\sigma-v)$ (for k=2 in (1)).

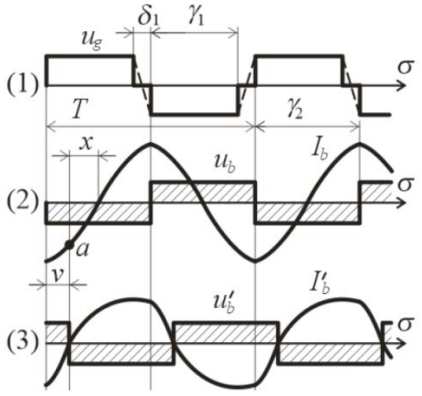

Fig. 3

The input voltage of the RPC rectifier $u'_b(t)$ is a function of its current $i_b(\sigma)$ and at small zero pauses $\delta\to 0$ is defined as follows

$$u_b(\sigma) = U_q \operatorname{sgn}(i_b(\sigma))\Big|_{|i_b(\sigma)|>i_0}, \quad \text{or} \quad u_b(\sigma) = 0\Big|_{|i_b(\sigma)|<i_0} \qquad (8)$$

where i_0 is a relatively small reverse current of the rectifier diodes. However, the conductivity intervals of the rectifier diodes γ_b in modes close to the idle one can decrease to zero and the pause will appear when the input voltage is less than the output voltage of the rectifier $|u_b|<U_q$. Therefore, in the future, it is advisable to investigate the limits of the change in the RPC load at $|u_b|\geq U_q$, when the presented quasi-static model of the RPC is valid.

Fig. 3 shows diagrams of the inverter voltage u_g (1), input current I_b, and rectifier input voltage u_b of the resonant converter at the uncoordinated phase (2) and at the coordinated phase u'_b and I'_b (3): here δ_1, γ_1 and γ_2 are relative values of the pause, pulse length of the inverter and rectifier, v is the variable offset. For the processes in Fig. 3, it can be established that since the current I_b is out of phase with the voltage u_g, the RPC operates in the high-frequency range of the operating frequency ($\omega_g>\omega_0$). At ***a*** point**,** the current I_b was negative in its initial position, and when the voltage of the second equivalent generator is shifted to the right by the value v $u'_b(\sigma) = u_b(\sigma-v)$, the current has shifted by some value x and at the same time becomes zero and shifted relative to the beginning of the period also by the value v: $I_b(\sigma - v)$. In this case, the partial derivative of the steady-state current at the point where the voltage passes through zero (σ = v) will be positive. RPC studies have shown that in the low-frequency range of the operating frequency ($\omega_g < \omega_0$) the derivative of the steady-state current at this point will be negative.

Therefore, the conditions for matching the voltage phase of the k-th equivalent generator for the general case according to the above considerations can be expressed as follows

$$I_{sk}(v-x_k)=0 \quad \text{with} \quad x_k \to v, \qquad \frac{\partial}{\partial v} I_{sk}(v-x_k) < 0 \quad \text{or} \quad \frac{\partial}{\partial v} I_{sk}(v-x_k) > 0 \qquad (9)$$

for the low operating frequency range or for the high operating frequency range, respectively. The desired variable offset of the input voltage of the RPC rectifier relative to the initial value is determined from the solution of equation (9) by numerical methods within certain limits of the variable v under the following calculation conditions:

- v=0.1...0.6, $\frac{\partial}{\partial v} I_{sB}(v-x_k) < 0$ in the low operating frequency range $0.5\cdot\omega_0<\omega_g<\omega_0$;
- v=0...0.5, $\frac{\partial}{\partial v} I_{sB}(v-x_k) > 0$ in the high operating frequency range $\omega_0<\omega_g<2\cdot\omega_0$.

Fig. 4, *a* and Fig. 4, *b* show the diagrams of relative shifts $\sigma(q,\omega^*_g)$ between the initially in-phase voltage pulses of the equivalent generators EG1 and EG2 of the replacement circuit in Fig. 1, *b* for the values of the LC-circuit Q = 2 and Q = 7, where the labels on the graphs correspond to the experimental data, graphs 1-7 correspond to the relative values of the output voltage: q=*0*.01; 0.05; 0.10; 0.25; 0.50; 0.65; 0.99

The arrays of values for the dependencies $\sigma(q,\omega^*_g)$ were calculated and interpolated by numerical methods for the relative values of the output voltage $q=U_q/U_s$ and the operating frequency $\omega^*_g = \omega_g/\omega_0$. The

matched offsets for the quasi-static model of the RPC are calculated for the low frequency range or for the high operating frequency range respectively: $v_a = 1-\sigma$ or $v_a = 0.5-\sigma$.

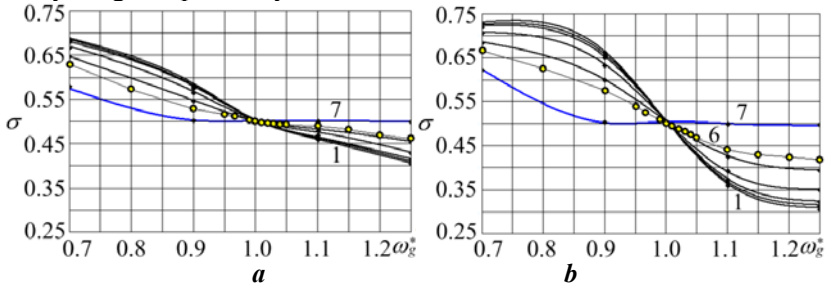

Fig. 4

4. Determination of the dependence of the steady-state rectifier current on the operating frequency range. Let's write down the expressions of steady-state currents at the output of the inverter and at the input of the rectifier for the RPC circuit in Fig. 1 according to (1) and (2) for the voltages of the inverter and rectifier in the form of diagrams *1* and *2* in Fig. 2, *a* with $k = 1$, $j = 2$, $x_j = x_{sB}$. The steady-state input current of the rectifier with the agreed phase for $x_{sB}=v$ will be as follows

$$I_{sB}(\sigma - x_{sB}) = I_{sB1}(\sigma - x_{B1}) \pm I_{sB2}(\sigma - x_{B2} - v), \tag{10}$$

where the "+" and "–" signs correspond to the low and the high operating frequency ranges.

The expressions of the components of the steady-state input current of the rectifier are as follows:

– inverter component: $(\sigma - x_{B1}) = U_s \cdot (\Phi_{B1}(\sigma, 0) - \Phi_{B1}(\sigma, \gamma_1) - \Phi_{B1}(\sigma, 0.5) + \Phi_{B1}(\sigma, 0.5+\gamma_1))$,

– rectifier component: $I_{sB2}(\sigma - x_{B1} - v) = U_q \cdot (\Phi_{B2}(\sigma, v) - \Phi_{B2}(\sigma, \gamma_2+v) - \Phi_{B2}(\sigma, 0.5+v) + \Phi_{B2}(\sigma, 0.5+\gamma_2+v-1))$, where x_{sB} is the resulting offset in the rectifier current caused by the shift v of its voltage; v is the variation shift; x_{21} and x_{22} are the initial offsets of the inverter and rectifier current components; U_s and U_q are the voltage amplitudes of equivalent generators. The stationary functions $\Phi_{B1}(\sigma,\delta)$ and $\Phi_{B1}(\sigma,\delta)$ in the formulas above are calculated by (7) for $\delta = 0$; γ_1; 0.5; $0.5+\gamma_1$ (inverter component) and for $\delta = v$; $v+\gamma_2$; $0.5+v$; $0.5+v+\gamma_2-1$ (rectifier component). A unit is also subtracted from the last offset if, when shifted to the right by v, this voltage step goes beyond the current operating frequency period, which must be taken into account when building calculation formulas in symbolic computing software applications.

5. Calculation of the average rectifier current. The average rectifier current I_q passing through the parallel-connected filter capacitance C_q and load resistance R_q in Fig. 1, *a* is closer to the steady-state load current, the greater is the filtering time constant C_qR_q. In the quasi-static model, the average output current can be determined by integrating the current at the non-zero voltage intervals of the *k*-th equivalent generator

$$I_q = \mp 2 \cdot \int_{v}^{v+\gamma_k} I_{sk}(\sigma - x_{sk}) d\sigma, \tag{11}$$

where the signs "–" and "+" correspond to the low and the high operating frequency ranges. Multiplication by 2 means a double current flow during the operating frequency period through the output equivalent generator with the symmetrical rectangular voltage shown in Fig. 2, *a*. The average current of the RPC rectifier is calculated over the conductivity intervals of the rectifier diodes. For a conditionally continuous current, we can take $\gamma_b = 0.5$.

It should be noted that when the phase of the output equivalent generator is matched, it operates only as an energy receiver. If the RPC rectifier consists of fully controlled switches with bilateral conductivity, for example, CMOS transistors [21, 22], then the conductivity intervals of the rectifier switches and the integration intervals in (11) may not depend on the input current of the rectifier and then the phase of the output equivalent generator will be set by the transistors switching algorithm, depending on which the output equivalent generator will be able to receive and deliver energy in interaction with the passive part of the RPC replacement circuit.

6. Experimental verification of the quasi-static model. The quasi-static model of the RPC does not take into account the nonlinearity of the power circuit and some parasitic parameters [23]. Comparison of the calculation results obtained using the idealized quasi-static model with the experimental characteristics obtained using a real RPC sample may contain a significant proportion of unaccounted-for factors, which will interfere with the comparative analysis. Therefore, at this stage of the research, it was decided to use simulation modelling, in which both the quasi-static mathematical model and the simulation model of the

RPC can take into account the same assumptions and thus reduce the factors of differences caused by different input data.

Table shows the diagrams of the stationary processes of the RPC in Fig. 1, *a*, obtained in different ways. The left column of the diagrams is obtained as a result of calculations of the quasi-static model in the *MathCAD* software application. The right column of the diagrams is obtained as a result of simulation modelling with a *SIMULINK* model similar to the models [2, 20] for five values of the relative operating frequency ω^*_g. Here the lines *a*, *b*, *c*, *d*, *e* correspond to ω^*_g=0.80, 0.95, 1.00, 1.05, 1.25. In Table the diagrams *1* and *2* are the voltages of the inverter u_g and rectifier u_b, *3* is the rectifier current I_{sB}, *4* is the current component from the inverter I_{sB1}, 5 is the current component from the rectifier I_{sB2}.

	Theoretical calculation	Model experiment
a	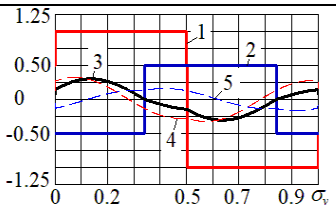	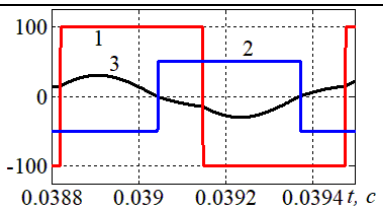
b	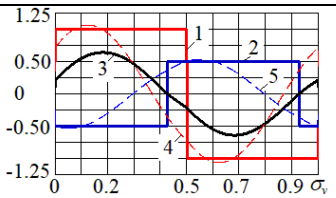	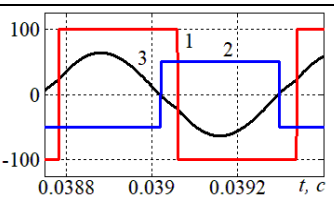
c	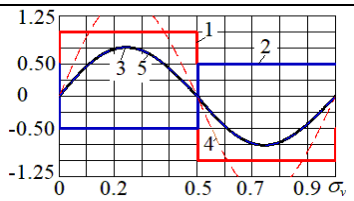	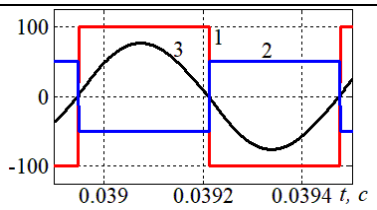
d	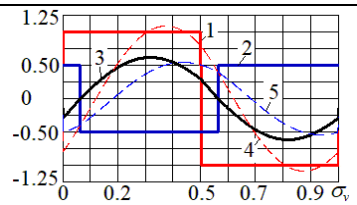	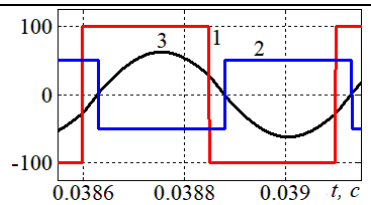
e	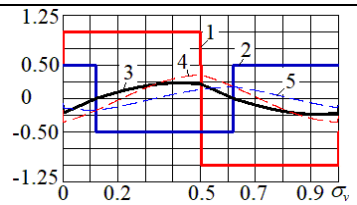	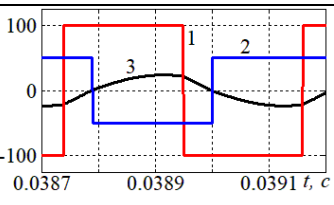

The calculation of the values was performed in relative units for the supply voltage U_s = 1 V and the load voltage U_q= 0.5 V. The simulation was performed for U_s = 100 V and U_q = 50 V. The circuit parameters are as follows: R = *0*.837 Ohm; L = 0.7 mHn; C= 10 μF; Q = *10*; resonant frequency f_0 = 1902.27 Hz; operating frequency was set to f_g = 1521.8 Hz; 1807.16 Hz; 1902.27 Hz; 1997.38 Hz; 2377.8 Hz.

The graphs of the processes in the left and right columns of Table were obtained in different ways, but they are visually identical. The difference between the results of theoretical calculations and modeling, reduced to an equal scale, did not exceed ±1.5%. Comparisons were also made for other modes of RPC operation, which also showed good convergence.

Based on practical experience, it can be assumed that the simulation model of the RPC reliably reproduces its processes. Thus, the convergence of the results of theoretical calculations and simulation modeling results indicates the adequacy of the quasi-static RPC model.

7. Results of calculating static characteristics. Fig. 5 and Fig. 6 show examples of the static characteristics of the RPC with the circuit in Fig. 1, *a* and with the diode rectifier, which were calculated by numerical methods using the quasi-static model for the structural replacement circuit in Fig. 1, *b* and for the following input parameters: L=1 Hn, C=1 F, Q = 2, Q = 7, ω_0 = 1 rad/s for relative load voltage q=*0*.5, 0.2, 0.1 in Fig. 5, *a-b* (control characteristics) and relative operating frequency ω^*_g= 1.01; 1.05; 1.10; 1.20; 2.00 in Fig. 5, *c-d* (dependence of efficiency on the relative load voltage q). The relative operating frequency was taken to be in the range of ω^*_g = 1.0...2.0. The supply voltage is assumed to be constant U_s = 100 V. The load is represented by a constant voltage source that was set within U_q = 0...100 V.

The load characteristics of the RPC in Fig. 6, *a-b* are nonlinear and sensitive to the circuit quality factor. Here (see Fig. 6) are the load characteristics of the RPC for Q-factor values Q=*2* (graphs with indices *a)* and Q=7 (graphs with indices *b)* and for relative operating frequency ω^*_g=1.25, 1.20, 1.10, 1.05, 1.01 (graphs *1*, *2*, *3*, *4*, *5*); labels indicate experimental data. Within the calculations close to the resonant frequency, an approximately proportional dependence of the maximum load currents on the circuit quality factor is observed. This is consistent with the phenomenon of resonant increase in the amplitudes of oscillations in the RPC circuit. Also, the higher the circuit quality factor, the greater the multiplicity of load current control.

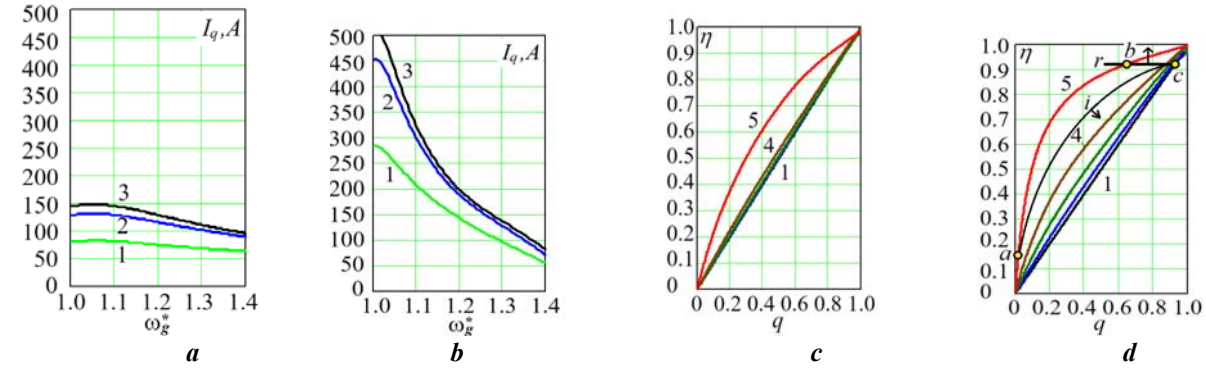

Fig. 5

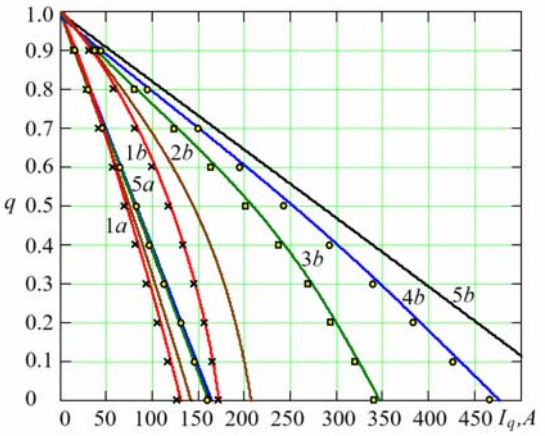

Fig. 6

The dependences of the RPC efficiency on the relative load voltage in Figs. 5, *c-d* (for Q-factors Q=2 and Q=7; graphs *1-5* for ω^*_g = 1.01, 1.05, 1.10, 1.20, 2.00) demonstrate the limits of the achievable RPC efficiency at different operating frequencies. When the output current I_q=const is stabilized, a set of points corresponding to certain different values of the operating frequency and load voltage form a constant-current control trajectory *i* on the field of efficiency dependencies (see Fig. 5, *d*). The resistive load corresponds to the trajectory *r*. For example, if you set the range of control of the relative operating efficiency in the RF range ω^*_g=1.01...2.0, then the control trajectory *i* for a constant current I_q = 50 A between points *a* and *c* or the control trajectory *r* for a constant resistance R_q = 2 Ohm between points *b* and *c* in Fig. 5, *d* for Q = 7 will be used. The arrows show the direction of the control trajectories offset with increasing current and load resistance.

The dependences of the relative load voltage on the load current of the RPC in Fig. 6 (indices of graphs *a* and *b* for Q-factor Q = 2 and Q = 7; graphs *1-5* for ω^*_g=1.25, 1.20, 1.10, 1.05, 1.01) approach linear when the operating frequency approaches the resonant frequency. This indicates a change in the nature of the passive part output impedance from reactive to active and is consistent with changes in the output voltage of the resistive load during frequency control. The cross-shaped labels correspond to the experimental data at ω^*_g=1.25, the square labels – at ω^*_g=1.10, the round labels – at ω^*_g=1.05. The experiments were carried out with the *SIMULINK* model of the RPC with the diode rectifier [2], which takes into account the voltage drop across the diodes of the rectifier of 0.75 V and diode leakage currents of 1 mA/V. The data for static characteristics were determined as the average current values in the sections of the time diagrams where the transients were considered to be completed. The experimental points in Fig. 6 are mostly located below the corresponding theoretical characteristics. This occurs due to the voltage drop of two diodes of the bridge rectifier, which was not taken into account by the theoretical quasi-static model. The location of the experimental points on the graphs demonstrates that the experimental data correspond to close to theoretical regularities. Therefore, this also confirms the adequacy of the quasi-static model of the RPC.

Conclusions. As a result of this study, an idealized quasi-static model of the resonant power converter was created, which allows to calculate the static characteristics. The worth of the theoretical characteristics lies in demonstrating the maximum capabilities of the resonant converter power circuit with

possible improvements in the parameters of the power circuit components and with appropriate transistors switching algorithms.

In the quasi-static model, it is possible to consider indirectly the nonlinear characteristics of power components by the experimental and analytical method. In this case, the transient functions $g_{kj}(s)$ of the passive part of the circuit are determined by the identification procedures [20, 24] from the experimental transient characteristics at different amplitudes of step impacts. Thus, the created quasi-static model during the transient functions $g_{kj}(s)$ correction in accordance with the available passive part can be used to calculate the characteristics of converters similar in principle of operation.

The work was performed within the framework of the state budget research: "Development of energy-efficient means of generating and converting electricity for small ship demagnetization systems"

1. Dymerets A.V., Yershov R.D., Gorodny A.N., Revko A.S., Denisov Y.O. Control characteristics of zero-current-switching quasi-resonant buck converter under variation of resonant circuit and load parameters. IEEE EUROCON 19th International Conference *on Smart Technologies*, Lviv, Ukraine, 06-08 July 2021. Pp. 443-448. DOI: https://doi.org/10.1109/EUROCON52738.2021.9535597.

2. Pavlov G.V., Obrubov A.V., Vinnichenko I.L., Makhnov A.O. Calculation of the regulatory characteristics of resonant converters by the superposition method. *Tekhnichna Elektrodynamika*. 2024. No 4. Pp. 24-33. (Ukr) DOI: https://doi.org/10.15407/techned2024.04.024.

3. Dymerets A.V., Yershov R.D., Gorodny A.N., Revko A.S., Savchenko D., Lytvyn S.V. Static characteristics of zero-current-switching quasi-resonant buck converter under variation of resonant circuit and load parameters. IEEE 41st International Conference on *Electronics and Nanotechnology (ELNANO)*, Kyiv, Ukraine, 10-14 October 2022. Pp. 721-727. DOI: https://doi.org/10.1109/ELNANO54667.2022.9927073.

4. Pavlov G., Obrubov A., Vinnychenko I. Design procedure of static characteristics of the resonant converters. IEEE 3rd Ukraine Conference on *Electrical and Computer Engineering (UKRCON)*, Lviv, Ukraine, 26-28 August 2021. Pp. 401-406. DOI: https://doi.org/10.1109/UKRCON53503.2021.9575698.

5. Ninomiya T., Higashi T., Harada K., Tsuya N., Gohnai T., Honda Y. Analysis of the static and dynamic characteristics of push-pull parallel resonant converters. *17th Annual IEEE Power Electronics Specialists* Conference. Vancouver, Canada, 23-27 June 1986. Pp. 367-374. DOI: https://doi.org/10.1109/PESC.1986.7415583.

6. Firmansyah E., Tomioka S., Abe S., Shoyama M., Ninomiya T. Steady state characteristics of active-clamped full-wave zero-current-switched quasi-resonant boost converters. IEEE 6th International *Power Electronics and Motion Control* Conference. Wuhan, China, 17-20 May 2009. Pp. 556-560. DOI: https://doi.org/10.1109/IPEMC.2009.5157449.

7. Pavlov G., Vinnichenko I., Pokrovskiy M. Research of the interrelationship between the frequency converter on the basis of the resonant inverter with nonlinear control power unit parameters and its load. IEEE First Ukraine Conference on *Electrical and Computer Engineering (UKRCON)*, Kyiv, Ukraine, 29 May – 02 June 2017. Pp. 554-559. DOI: https://doi.org/10.1109/UKRCON.2017.8100300.

8. Pavlov G.V., Vinnichenko I.L., Obrubov A.V. Frequency converter with the reduced thd of the output voltagel. *Tekhnichna Elektrodynamika*. 2016. No 5. Pp. 14-16. (Ukr) DOI: https://doi.org/10.15407/techned2016.05.014.

9. Pavlov G., Vinnichenko I., Pokrovskiy M. Estimation of energy efficiency of the frequency converter based on the resonant inverter with pulse-density control. IEEE 3rd International Conference on *Intelligent Energy and Power Systems (IEPS)*, Kharkiv, Ukraine, 10-14 September 2018. Pp. 101-105. DOI: https://doi.org/10.1109/IEPS.2018.8559499.

10. Martin-Ramos J.A., Diaz J., Pernia A.M., Lopera J.M., Nuno F. Dynamic and steady-state models for the PRC-LCC resonant topology with a capacitor as output filter. *IEEE Transactions on Industrial Electronics*. 2007. Vol. 54. No 4. Pp. 2262-2275. DOI: https://doi.org/10.1109/TIE.2007.894763.

11. Chandwani A., Mallik A., Akturk A. Steady-state model-derived multivariable loss optimization for triple active C^3L^3 resonant converter. *IEEE Transactions on Transportation Electrification*. 2024. Vol. 10. No 1. Pp. 1729-1746. DOI: https://doi.org/10.1109/TTE.2023.3266744.

12. Introduction to Resonant Converters. URL: https://www.monolithicpower.com/en/learning/mpscholar/isolation-solutions/llc-converters/introduction-to-resonant-converters?srsltid=AfmBOoolNYDb_cuNO9IEJaRocOJVkdvY3WJVYckiNdefDCQdB10Uh07T (accessed at 25.12.2024)

13. Adragna C. LLC resonant converters: an overview of modeling, control and design methods and challenges. *Foundations and Trends® in Electric Energy Systems*. 2022. Vol. 5. No 2–4. Pp. 75-491. DOI: https://doi.org/10.1561/3100000029.

14. Lazar J.F., Martinelli R. Steady-state analysis of the LLC series resonant converter. *Sixteenth Annual IEEE Applied Power Electronics* Conference and Exposition. Anaheim, CA, USA, 04-08 March 2001. Vol. 2. Pp. 728-735. DOI: https://doi.org/10.1109/APEC.2001.912451.

15. Yang R., Ding H., Xu Y., Yao L., Xiang Y. An analytical steady-state model of LCC type series–parallel resonant converter with capacitive output filter. *IEEE Transactions on Power Electronics*. 2014. Vol. 29. No 1. Pp. 328-338 DOI: https://doi.org/10.1109/TPEL.2013.2248753.

16. Abdel-Rahman S. Resonant LLC Converter: Operation and Design. Infineon Technologies North America (IFNA) Corp. 2012. Pp. 1-19. URL: https://www.infineon.com/dgdl/Application_Note_Resonant+LLC+Converter+Operation+and+Design_Infineon.pdf?fileId=db3a30433a047ba0013a4a60e3be64a1. (accessed at 25.12.2024)

17. Kundu U., Sensarma P. A unified approach for automatic resonant frequency tracking in LLC DC–DC Converter. *IEEE Transactions on Industrial Electronics*. 2017. Vol. 64. No 12. Pp. 9311-9321. DOI: https://doi.org/10.1109/TIE.2017.2711520.
18. He R., Wang H., Xue B. Automatic resonant frequency tracking scheme for LLC resonant converter based on adaptive extended state observer. *IEEE Applied Power Electronics* Conference and Exposition *(APEC)*, Houston, TX, USA. 20-24 March 2022. Pp. 22-26. DOI: https://doi.org/10.1109/APEC43599.2022.9773470.
19. Pavlov G., Obrubov A., Vinnichenko I. Optimizing the operation of charging self-generating resonant inverters. *Eastern-European Journal of Enterprise Technologies*. 2022. Vol. 1. No 5(115). Pp. 23-34. DOI: https://doi.org/10.15587/1729-4061.2022.252148.
20. Pavlov G., Obrubov A., Vinnichenko I. Determining the dynamic model of the charging resonant converter with inductive coupling by an experimental-analytical method. *Eastern-European Journal of Enterprise Technologies*. 2022. Vol. 4. No 8(118). Pp. 17-28. DOI: https://doi.org/10.15587/1729-4061.2022.263526.
21. Wang Z.C., Wang D.Y., Zhan Z.J., Wang B.C., Jia L.J. Analysis and design of an LCC resonant current-source power supply for PFU charging applications. *IEEE Pulsed Power* Conference *(PPC)*. Austin, TX, USA, 31 May – 04 June 2015. Pp. 1-6. DOI: https://doi.org/10.1109/PPC.2015.7296942.
22. Chen X., Batarseh I. A fixed switching frequency dual-input LLC converter with PWM controlled semi-active rectifiers for PV applications. *IEEE Applied Power Electronics* Conference and Exposition *(APEC)*. Phoenix, AZ, USA. 14-17 June 2021. Pp. 320-326. DOI: https://doi.org/10.1109/APEC42165.2021.9487039.
23. Koscelnik J., Sedo J., Dobrucky B. Modeling of resonant converter with nonlinear inductance. *International Conference on Applied Electronics*. Pilsen, Czech Republic. 09-10 September 2014. Pp. 153-156. DOI: https://doi.org/10.1109/AE.2014.7011689.
24. Voitenko V.P. Algorithm stages of quasi-optimal regulation in system with a pulse converter. *Tekhnichna Elektrodynamika*. 2012. No 3. Pp. 125-126. URL: https://previous.techned.org.ua/2012_3/st60.pdf. (Rus.)

УДК 621.314

КВАЗІСТАТИЧНА МОДЕЛЬ РЕЗОНАНСНОГО ПЕРЕТВОРЮВАЧА ЕЛЕКТРОЕНЕРГІЇ

Г.В. Павлов, докт. техн. наук, **А.В. Обрубов**, докт. техн. наук, **І.Л. Вінниченко**, канд. техн. наук,
А.О. Махнов
Національний університет кораблебудування імені адмірала Макарова,
пр. Героїв України, 9, Миколаїв, 54007, Україна.
E-mail: pavlov.gv.nuk@gmail.com; andrii.obrubov@nuos.edu.ua; i.l.vinnychenko@gmail.com; andrei.schneidereu@gmail.com.

Розроблено квазістатичну модель резонансного перетворювача електроенергії з двохтактним інвертором, LLC-контуром і діодним випрямлячем, яка представляє собою лінійну математичну модель, отриману на основі аналізу квазісталих процесів схеми заміщення для постійних значень вхідних і вихідних величин. Квазістатична модель визначена на основі динамічної моделі резонансного перетворювача для нескінченного часу, що дало змогу одержати аналітичні вирази статичних характеристик на основі перехідних функцій. В результаті розрахунків за квазістатичною моделлю маємо сімейства статичних характеристик резонансного перетворювача, який заміщується структурою з еквівалентними генераторами напруги і пасивною частиною схеми. Пасивна частина містить резонансний контур, трансформатор напруги і деякі паразитні параметри трансформатора та інших елементів схеми. Еквівалентні генератори напруги заміщують інвертор напруги з джерелом живлення і випрямляч з навантаженням. Таким чином, комутована силова схема резонансного перетворювача заміщується некомутованою схемою з генераторами напруги і пасивним багатополюсником. Вхідними величинами схеми заміщення є напруги еквівалентних генераторів, а їхні струми – вихідними величинами. Квазісталі процеси представлено як сукупність стаціонарних функцій, що складаються зі стаціонарних перехідних функції. Стаціонарні функції є сумою окремих перехідних функцій, які повторюються із періоду в період робочої частоти. Задля визначення перехідних функцій за теоремою про кінцеве значення z-зображення використано передатні функції, отримані із дискретної динамічної моделі резонансного перетворювача. Алгоритм комутації силових вентилів враховується під час складання формули стаціонарного струму вихідного еквівалентного генератору, на проміжках ненульової напруги якого за допомогою інтегрування стаціонарного струму визначається середній струм навантаження. Порівняння розрахованих статичних характеристик з експериментальними підтвердило правильність теоретичних результатів. Бібл. 24, рис. 6, табл. 1.

Ключові слова: резонансний перетворювач, квазістатична модель, стаціонарна функція, перехідна функція.

Received 06.01.2025
Accepted 10.04.2025